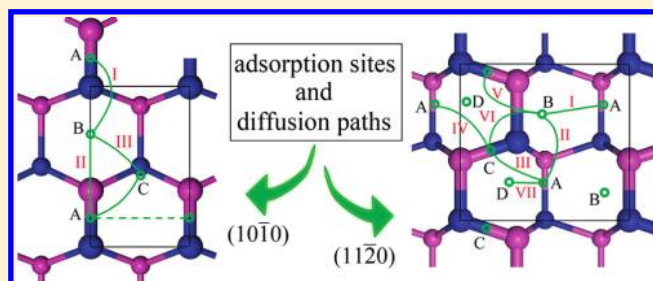


# Structural and Electronic Properties of the Adsorption of Oxygen on AlN ( $10\bar{1}0$ ) and ( $11\bar{2}0$ ) Surfaces: A First-Principles Study

Honggang Ye,\* Guangde Chen, and Yelong Wu

Department of Applied Physics and the MOE Key Laboratory for Nonequilibrium Synthesis and Modulation of Condensed Matter, Xi'an Jiaotong University, Xi'an, 710049, People's Republic of China

**ABSTRACT:** By using first-principles calculation methods, the structural and electronic properties of the adsorption of oxygen on wurtzite AlN ( $10\bar{1}0$ ) and ( $11\bar{2}0$ ) surfaces are investigated. Atomic adsorption is supposed to be the main adsorption morphology for both surfaces because it is more stable in energy than molecular adsorption and  $O_2$  can dissociate easily during access to the surfaces. The stable adsorption sites on the two surfaces are not unique but the diffusions of O adatoms between them are limited by high energy barriers. The spin polarization of the triplet O and  $O_2$  is relieved after adsorption. Detailed analysis of the electronic band structures shows that the adsorbates tend to drive away the original surface states from the bulk band gap but introduce into oxygen related states.



to drive away the original surface states from the bulk band gap but introduce into oxygen related states.

## 1. INTRODUCTION

Group III-nitrides are widely used for blue and ultraviolet optoelectronics as well as high-power radio frequency electronics. In addition to GaN, InGaN, and AlGaIn, special attention has been paid to the AlN binary compound due to its large band gap, high thermal conductivity, small thermal expansion coefficient, and other excellent physical properties.<sup>1–4</sup> It can be used as a wide band gap semiconductor for UV emitters, lasers, and high-mobility transistors, and can also be used as a substrate or buffer layer for the growth of III-nitrides and their alloys. As the nonpolar ( $10\bar{1}0$ ) and ( $11\bar{2}0$ ) surfaces have a low formation energy, increasing efforts have been aimed at the growth of AlN nonpolar films on the two planes to avoid the large polarization field in polar films.<sup>5,6</sup> In addition, the two facets often present as the lateral surfaces of AlN nanowires and nanotubes<sup>7–9</sup> and as the main component of the inner surfaces of some extended defects, such as nanopipes and cracks, which are generally observed in AlN epitaxial films.<sup>10–12</sup> Detailed study of the structural and electronic properties of the two surfaces is thus necessary for both film growth and further application and is helpful to understand the properties of the nanostructures and defects.

Oxygen is usually one of the unintended impurities adsorbed on the surfaces or incorporated into the lattice of AlN. At low concentration, the incorporated oxygen atoms sit at the N-sites<sup>13</sup> and behave as deep donors.<sup>14</sup> But an increase in concentration has great influence on the morphology of AlN films,<sup>15,16</sup> the sintering properties of AlN powders,<sup>17,18</sup> and the thermal conductivity and optical properties of AlN.<sup>18–20</sup> Works about the oxygen employed surfaces of AlN are confined in the polar (0001) and (000 $\bar{1}$ ) surfaces. The adsorption sites, binding energies, and electronic structures have been thoroughly discussed.<sup>21,22</sup> With the enhancement of interest in

nonpolar films and nanostructures, investigation of the interaction of oxygen with the nonpolar surfaces is expected. A recent work has reported a stable structure of oxygen incorporated complex defect on the AlN ( $10\bar{1}0$ ) surface,<sup>23</sup> which was also found to be responsible for the formation of nanopipes in AlN and GaN films.<sup>24,25</sup> As the melting temperature of AlN is high ( $\sim 2500$  K), the surface and volume diffusion of oxygen was reported to be very limited,<sup>15</sup> which implies that the adsorbed oxygen atoms mainly stay on the surface. Therefore, investigation of the adsorption structures and properties is meaningful. In this work, we investigated the adsorption of oxygen on AlN ( $10\bar{1}0$ ) and ( $11\bar{2}0$ ) surfaces by spin-unrestricted first-principles calculations. The possible adsorption geometries for both atomic and molecular oxygen, the adsorption energy and its dependence on coverage, the possible diffusion paths for O adatoms ( $O_{ad}$ 's), the reaction process of  $O_2$  with the surfaces, as well as the influence of adsorbate on surface electronic structure are concerned.

## 2. COMPUTATIONAL DETAILS

Density functional theory calculations are performed within the generalized gradient approximation (GGA)<sup>26</sup> framework as implemented by the Vienna Ab initio Simulation Package (VASP) code.<sup>27,28</sup> The spin is unrestricted since both atomic and molecular oxygen have a triplet group state. We employ Vanderbilt ultrasoft pseudopotentials.<sup>29</sup> The energy cutoff for the plane wave basis function is 500 eV. We employ a Monkhorst-Pack sampling scheme with a density of  $5 \times 8 \times 1$  k-point mesh for the ( $1 \times 1$ ) ( $10\bar{1}0$ ) surface and  $5 \times 5 \times 1$  for the ( $1 \times 1$ ) ( $11\bar{2}0$ ) surface.<sup>30</sup>

Received: June 9, 2010

Revised: December 22, 2010

Published: January 12, 2011

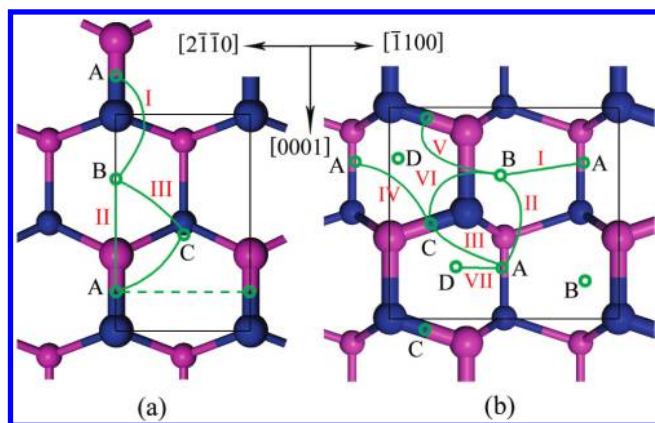


**Figure 1.** (Color online) Top views of the stick-ball models of AlN (10 $\bar{1}0$ ) (a) and (11 $\bar{2}0$ ) (b) surfaces. The N (blue) and Al (pink) atoms are distinguished by color and the atoms in first (large) and second (small) layers are distinguished by size. The green circles (denoted by A, B, C, D) and curves (numbered by I, II, III...) represent the possible adsorption sites and diffusion paths.

The slab models are built containing 16 and 11 atomic layers, respectively, for the (10 $\bar{1}0$ ) and (11 $\bar{2}0$ ) surface with a 12 Å vacuum space separating the slabs. The adsorbates are always equally added on both sides of the slabs. The top four layers for the (10 $\bar{1}0$ ) surface models, and three for (11 $\bar{2}0$ ), at both side of the slabs and any adsorbates are allowed to relax by minimizing the quantum mechanical force on each ion to be less than 0.03 eV/Å. The other layers are fixed in the optimized bulk configuration. The lattice parameters used in building the slab models are derived by optimizing the bulk primitive cell. Test calculations show that the cell size is converged. The minimum energy path (MEP) for  $O_{ad}$  to diffuse between the possible adsorption sites and the reaction process of  $O_2$  with AlN surfaces are probed by the nudged elastic band (NEB) method.<sup>31</sup>

The adsorption energy per oxygen atom is defined by the equation of  $E_{ads} = -(1/n)(E_{total} - E_{ref} - (n/2)E_{O_2})$ , where  $E_{total}$  and  $E_{ref}$  are the total energy of the adsorbed model and the responding relaxed clean surface model,  $E_{O_2}$  the energy of a free  $O_2$  molecule, and  $n$  the number of adsorbed oxygen atoms.

### 3. RESULTS AND DISCUSSION

The wurtzite AlN (10 $\bar{1}0$ ) surface is characterized by Al–N dimers along the  $c$  direction, with one dimer in each unit cell. The (11 $\bar{2}0$ ) surface is characterized by Al–N chains, with two N and two Al atoms in each unit cell. Top views of them are shown in Figure 1. The relaxation mode and electronic property of the clean (10 $\bar{1}0$ ) and (11 $\bar{2}0$ ) surfaces are well-known.<sup>32–34</sup>

**3.1. Adsorption on the (10 $\bar{1}0$ ) Surface.** The possible adsorption sites are explored by performing geometric optimization calculations for several typical adsorption models. The two sites denoted by A and B in Figure 1(a) are finally obtained for the (1 × 1) (10 $\bar{1}0$ ) surface. Site A lies above the Al–N dimer with an adsorption energy of 0.79 eV/atom, and site B lies between adjacent dimers in the  $c$  orientation, whose adsorption energy is 0.74 eV/atom. When both sites are occupied by O atoms at the same time, viz., two monolayer (ML) coverage, the average adsorption energy increases to 0.91 eV/atom. When the coverage decreases to 0.5 ML, with one  $O_{ad}$  in a (2 × 1) cell, sites A and B are still possible adsorption sites but their adsorption energies increase to 1.05 and 0.92 eV/atom, respectively. The coverage

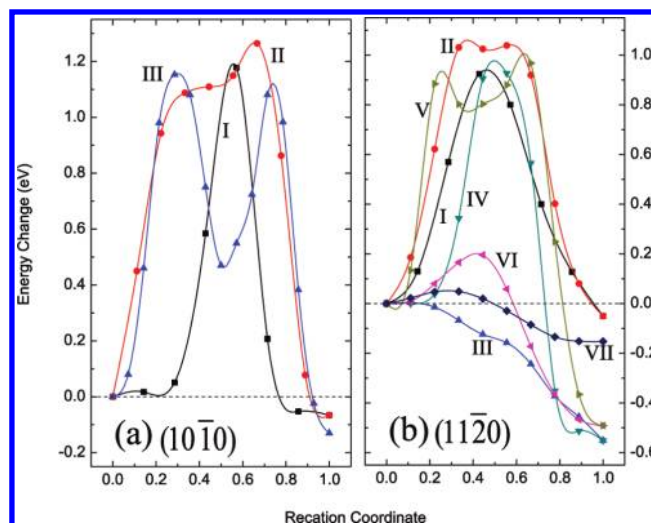


**Figure 2.** (Color online) The energy changes of the MEPs as a function of the reaction coordinate. The scatters are the energies of the NEB images.

dependence of adsorption energy indicates that there is an attractive interaction between the adjacent  $O_{ad}$ 's parallel to the dimer direction but a repulsive interaction perpendicular to the dimer direction. The  $O_{ad}$ 's thus prefer to dispose in lines along the dimer direction. In addition, another adsorption site, denoted by C in Figure 1(a), is found for the (2 × 1) reconstruction, at which the  $O_{ad}$  bonds with two Al atoms at the surface. Its adsorption energy is 0.45 eV/atom, much lower than those of sites A and B.

The possible MEPs for  $O_{ad}$ 's to diffuse between these sites are schematically revealed by the green lines in Figure 1(a) and their energy changes are shown in Figure 2(a). The  $O_{ad}$  at site B can diffuse to site A by either path I or II (step across a N or Al atom). The energy barriers of both paths are very high, about 1.17 and 1.26 eV, which indicates that the diffusion is difficult. We further considered whether site C can act as a middle state for the diffusion between sites A and B at 0.5 ML coverage, viz., along the path III. The result is unexpected. The energy barrier is considerable to that of path I. The depth of the valley in this curve, corresponding to site C, is 0.61 eV. It indicates that the  $O_{ad}$  at site C escapes relatively easily. Lymperakis et al.<sup>35</sup> reported that the Ga adatom on GaN (10 $\bar{1}0$ ) surface can diffuse easily perpendicular to the dimer direction (as the dashed line in Figure 1(a)) because only bond angle changes are involved in this process. However, similar diffusion is yet difficult for the  $O_{ad}$ 's on the AlN surface. The  $O_{ad}$  first experiences the N–O bond break and then is trapped at site C. The  $O_{ad}$  cannot reach the midst of two A sites without breaking the coordinated bonds. So we can deduce that the short lengths and strong strengths of N–O and Al–O bonds are the origins of the hard diffusion for  $O_{ad}$  on AlN (10 $\bar{1}0$ ) surface.

For the molecular adsorption, two final geometries with  $O_2$  lying parallel to the Al–N dimer and centering approximately at sites A and B, respectively, are obtained for the (1 × 1) cell. Their adsorption energies are 0.40 and 0.59 eV/atom, respectively. For the models with one  $O_2$  adsorbing on the (2 × 1) cell, three final adsorption geometries are obtained and schematically shown in Figure 3. It can be seen that the molecules approximately adsorb at the same sites as atomic oxygen. The centers of  $O_2$  in Mole1, Mole2, and Mole3 are close to sites A, B, and C in Figure 1(a), respectively. Their adsorption energies are 0.61, 0.67, and 0.55 eV/atom, respectively. It should be noted that Mole2 is the most stable

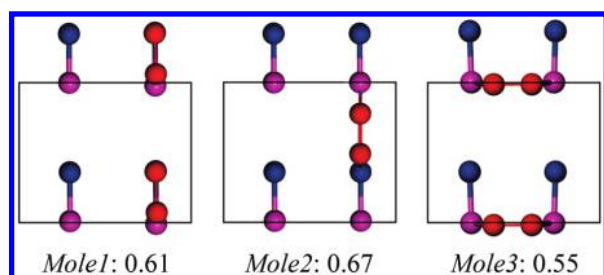


**Figure 3.** (Color online) Top views of the final geometries of  $O_2$  adsorbed ( $2 \times 1$ )  $(10\bar{1}0)$  surface. Only the top layer atoms of the substrate are presented. The N, Al and O atoms are presented by blue, pink, and red balls, respectively. Their adsorption energies (eV/atom) are listed below them.

configuration but not Mole1. Mole3 is the most unstable configuration here, but it was reported to be the most stable one for  $O_2$  adsorbing on ZnO  $(10\bar{1}0)$  surface.<sup>36</sup> This discrepancy can be approximately understood from the strength difference of the bonds between  $O_2$  and different surface species. It is known that the N–O bond is stronger than the O–O bond in general, so the total strength of N– $O_2$ –Al is stronger than Al– $O_2$ –Al but the O– $O_2$ –Zn is weaker than Zn– $O_2$ –Zn.

The molecular adsorptions are less stable in energy than the dissociative adsorptions, so we further considered whether  $O_2$  can dissociate during access to the  $(10\bar{1}0)$  surface. The reaction process is calculated by the NEB method.<sup>31</sup> It starts with a  $(2 \times 1)$  surface cell including an  $O_2$  lying far away from the surface ( $>5 \text{ \AA}$ ), and ends with dissociative O atoms adsorbing at two A sites. The change of energy for the process is revealed by the red line (circle symbols) in Figure 4(a). There is a transition state with an energy barrier of  $\sim 0.50 \text{ eV}$ . When the final state is changed to be with one O atom at site A and one at site B, the energy barrier decreases to  $0.02 \text{ eV}$  (triangle symbols). The small barriers indicate that the molecular oxygen can also result in atomic adsorption. Although molecular adsorption is found to be a barrier-free process (square symbols) by taking Mole2 in Figure 3 as an example, its probability is predicted to be small, especially at high temperature, because it is not energetically favored. Therefore, the main morphology of oxygen adsorption on the AlN  $(10\bar{1}0)$  surface is atomic adsorption, no matter whether the species in reservoir is molecular or atomic.

This consequence is absolutely different from the result for ZnO, for which molecular adsorption was found to be the unique format on the ideal  $(10\bar{1}0)$  surface.<sup>36</sup> An important factor of this difference is the more covalent nature of the Al–N bond. The surface N atom readily react to fill its vacant coordination site to reduce the surface energy. The stable atomic adsorption and difficult diffusion support the “hit and stick” mechanism advised by V. Brien et al.<sup>15</sup> which means that the oxygen atom stays on their impact site or at most a few atomic site away at AlN surface.

**3.2. Adsorption on the  $(11\bar{2}0)$  Surface.** There are always two equivalent sites in the  $(1 \times 1)$   $(11\bar{2}0)$  surface cell, so 1 ML coverage includes two  $O_{ad}$ 's per cell. For 0.5 ML coverage, three adsorption sites are found and denoted by A, B, and C in Figure 1(b). Sites A and B lie in the channel between Al–N chains, and site C lies above an N–Al bond. All of the  $O_{ad}$ 's at the three sites bond with the same central N atom. Their adsorption energies are 1.05, 1.00, and 0.50 eV/atom, respectively. When the coverage increases to 1 ML, the adsorption energies of sites A and B increase to 1.27 and 1.07 eV/atom, respectively, which indicates attractive interaction between the  $O_{ad}$ 's. The  $O_{ad}$  at site C now relaxes to site D, whose adsorption energy is 1.11 eV/atom, much larger than that of

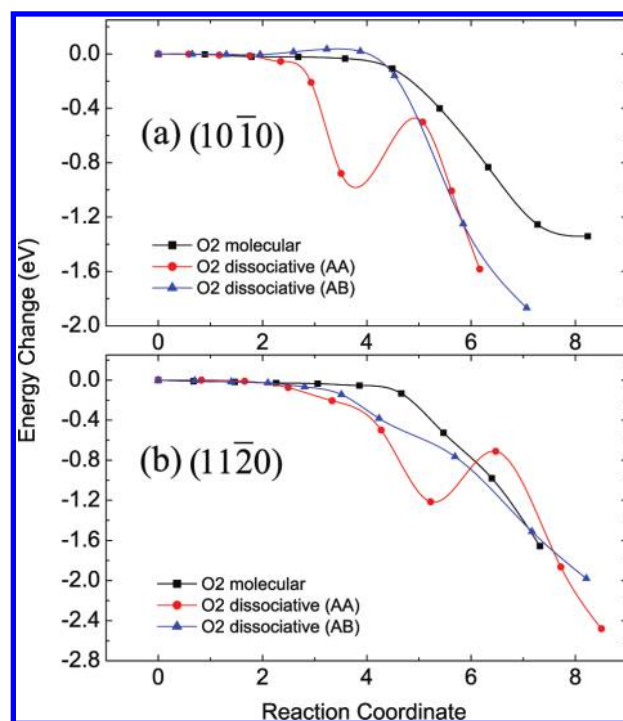


**Figure 4.** (Color online) The energy changes of the reaction processes of  $O_2$  adsorbing on the AlN  $(10\bar{1}0)$  (a) and  $(11\bar{2}0)$  (b) surfaces. The black (square) line is for molecular adsorption. The red (circle) and blue (triangle) lines are for dissociative adsorptions with O atoms at two A sites and A,B sites, respectively.

site C, but it does not exist at 0.5 ML coverage. The adsorption geometries of 1 ML coverage with one  $O_{ad}$  at site A and one at site B, one at site B and one at site D are also found, but the cooperation of sites A and D does not exist because of their short distance. A difference from the  $(10\bar{1}0)$  surface is that the  $O_{ad}$ 's at sites A, B, and D obviously embed in the  $(11\bar{2}0)$  surface, which induces apparent perturbation to the surface structure and large adsorption energy.

The possible diffusion paths for the  $O_{ad}$ 's on  $(11\bar{2}0)$  surface are revealed by the green lines in Figure 1(b), and the corresponding changes of energy along these paths are shown in Figure 2(b). The  $O_{ad}$  may diffuse from sites B to A by either path I or II, while they are forbidden by the high energy barriers. The  $O_{ad}$  at site C can diffuse to site A by either path III or IV. The barriers of the two paths, however, are absolutely different. The one of path IV is  $0.93 \text{ eV}$  while the one of path III is significantly smaller, about  $0.01 \text{ eV}$ . Similar results are obtained for the diffusion between sites B and C (path V and VI). The barrier from sites C to B along path V is  $1.01 \text{ eV}$ , while the one along path VI is  $0.19 \text{ eV}$ . At 1 ML coverage, the energy barrier to diffuse from sites D to A (path VII) is  $0.08 \text{ eV}$ . A whole feature is that the three paths with small barriers (III, VI, and VII) are all around the same surface N atom; any one to diffuse away from one central N atom to another is hard to occur. The diffusions along the three paths induce that only sites A and B are effective adsorption sites.

Two molecular adsorption geometries, shown in Figure 5, are found for the  $(11\bar{2}0)$  surface. Their adsorption energies are 0.84 and 0.68 eV/atom, lower than that of atomic adsorption. The calculation results of the reaction processes are similar to those of the  $(10\bar{1}0)$  surface.  $O_2$  can dissociate without or with small energy barriers (Figure 4(b)). Hence the main adsorption morphology is also atomic adsorption. The probability of molecular adsorption is small.

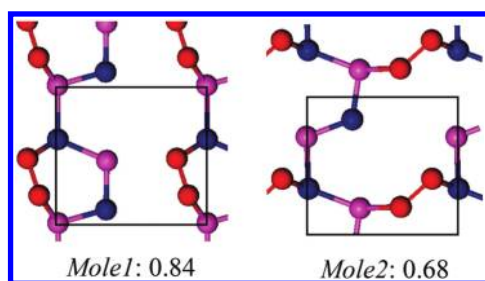


**Figure 5.** (Color online) Top views of the two final geometries of  $O_2$  adsorbed AlN (1120) surface. The N, Al, and O atoms are presented by blue, pink, and red balls, respectively. The adsorption energies (eV/atom) are given below each part.

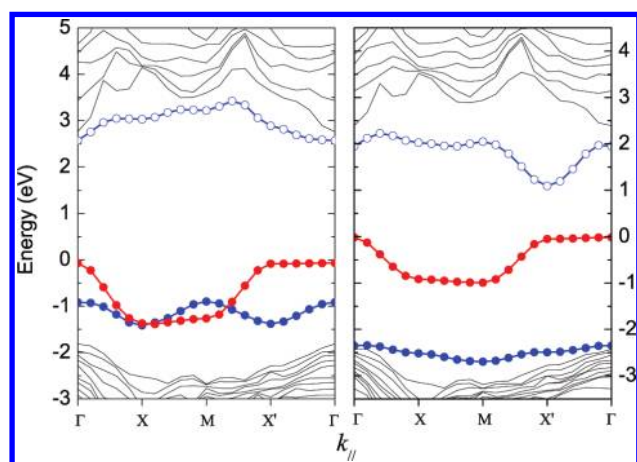


**Figure 6.** Energy band structures of the atomic (left) and molecular (right) adsorption of oxygen on AlN (1010) surface. The Fermi level is set to be zero.

**3.3. Influence on Electronic Structure.** The free O and  $O_2$ , however, are spin polarized in their ground states, they become nonspin polarized after adsorbing on the two surfaces. The degeneracy of the two atomic (molecular) orbitals which are occupied by unpaired electrons is relieved and no partially occupied orbital exists. The detailed electron configurations are discussed below.

The energy band structure of the model with  $O_{ad}$  at the site A of AlN (1010) surface is revealed in the left part of Figure 6. Three surface states appear in the bulk band gap. The one in the upper part of the band gap is empty and the other two ones are fully occupied. The clean (1010) surface introduces a filled surface state ( $S_N$ ) above the valence band maximum and an empty surface state ( $S_{Al}$ ) below the conduction band minimum, originating from the dangling bond of surface N and Al atom, respectively.<sup>33</sup> When covered by  $O_{ad}$ , two 2p orbitals ( $p_x, p_y$ ) of  $O_{ad}$  interact with the two surface dangling bonds, resulting in that the two surface states,  $S_N$  and  $S_{Al}$ , are pushed out of the band gap and an Al–O bonding state (filled blue circles) and N–O antibonding state (empty blue circles) are left in the lower and upper part of the bulk band gap. The state revealed by red circles is from the orbital  $p_z$  of  $O_{ad}$ , which cannot bond with the substrate because of symmetry mismatch. However, it has strong overlap with the nearest neighbor ones in the  $[2\bar{1}10]$  direction (perpendicular to the N–Al dimer), the corresponding band thus has a wide dispersion from the  $\Gamma$  to X point in the reciprocal space, which is parallel to the  $[2\bar{1}10]$  direction in the real space.

The energy band structure of the model with  $O_2$  adsorbing above the Al–N dimer of (1010) surface is revealed in the right part of Figure 6. There are also two occupied surface states and one empty surface state in the band gap but the origins of them are different.  $O_2$  has two unpaired electrons occupying two degenerate orbitals, which are classified as antibonding. Both of the two orbitals are parallel to the orientation of  $O_2$  but one is perpendicular to the surface ( $\pi_{\perp}^*$ ) and another is parallel to the surface ( $\pi_{\parallel}^*$ ). The molecular orbital  $\pi_{\perp}^*$  interacts with both dangling bonds of the surface Al and N, resulting in that the  $S_{Al}$  is pushed up into the conduction band and the  $S_N$  is pushed down but still maintains above the valence band maximum (filled blue circles) and the  $\pi_{\perp}^*$  finally lies in the upper part of the band gap (empty blue circles). The molecular orbital  $\pi_{\parallel}^*$  cannot bond with the surface dangling bonds because of symmetry mismatch but the interaction between the neighboring cells along the  $[2\bar{1}10]$  direction make the responding band have a wide dispersion, as shown by the red curve. The center of the band in red in the right part of Figure 6 is higher than that of the one in the left part. This fact agrees with the general conclusion that the energy of an antibonding state is higher than that of the corresponding atomic orbital.

The electronic structures of the other adsorbing geometries on the (1010) surface and the adsorbing geometries on the (1120) surface will not be discussed here in detail. They can be understood by the mechanisms discussed above for atomic and molecular adsorption, respectively. We can confirm that the adsorption of oxygen tends to drive away the surface states of the clean surface from the band gap but introduces oxygen-related states into the band gap.

## 4. CONCLUSIONS

The geometry and electronic properties of oxygen adsorption on AlN (1010) and (1120) surfaces are investigated by first-principles calculations. Atomic adsorption is energetically preferred for both surfaces and  $O_2$  can dissociate without or with small energy barriers during access to the surfaces. The probability of molecular adsorption is thus predicted to be small although some configurations of them are found. The stable adsorption sites on the (1010) surface dispose in lines above the Al–N dimers and parallel to the dimer orientation, and those on the (1120) surface lie in the channels between surface Al–N chains. Because of the short length and strong strength of N–O and Al–O bonds, the diffusion of  $O_{ads}$  on both surfaces is very limited. The spin polarization of triplet O and  $O_2$  is eliminated after adsorption. Detailed analysis of the energy band structures shows that the adsorbed O and  $O_2$  tend to drive out the original surface states from the bulk band gap but enter into oxygen related states.

## AUTHOR INFORMATION

### Corresponding Author

\*E-mail: yehonggang@stu.xjtu.edu.cn.

## ACKNOWLEDGMENT

The authors gratefully acknowledge the financial support of the Natural Science Fund of China (Grant No. 11074200) and the Natural Science Fund of Shaanxi Province (Grant No. 2009JM1005) and the computing support of the NHPCC at Xi'an.

## ■ REFERENCES

- (1) Raghavan, S.; Weng, X. J.; Dickey, E.; Redwing, J. M. *Appl. Phys. Lett.* **2005**, *87*, 142101.
- (2) Songmuang, R.; Landre, O.; Daudin, B. *Appl. Phys. Lett.* **2007**, *91*, 251902.
- (3) Sun, Q.; Wang, J. T.; Wang, H.; Jin, R. Q.; Jiang, D. S.; Zhu, J. J.; Zhao, D. G.; Yang, H.; Zhou, S. Q.; Wu, M. F.; Smeets, D.; Vantomme, A. *J. Appl. Phys.* **2008**, *104*, 043516.
- (4) Zhao, D. G.; Zhu, J. J.; Liu, Z. S.; Zhang, S. M.; Yang, H.; Jiang, D. S. *Appl. Phys. Lett.* **2004**, *85*, 1499.
- (5) Armitage, R.; Suda, J.; Kimoto, T. *Appl. Phys. Lett.* **2006**, *88*, 011908.
- (6) Haskell, B. A.; Nakamura, S.; DenBaars, S. P.; Speck, J. S. *Phys. Status Solidi B* **2007**, *244*, 2847.
- (7) Zhao, Q.; Zhang, H. Z.; Xu, X. Y.; Wang, Z.; Xu, J.; Yu, D. P.; Li, G. H.; Su, F. H. *Appl. Phys. Lett.* **2005**, *86*, 193101.
- (8) Wu, Y. L.; Chen, G. D.; Ye, H. G.; Zhu, Y. Z.; Wei, S.-H. *J. Appl. Phys.* **2008**, *104*, 084313.
- (9) Zhang, L.; Shi, J. J.; Tansley, T. L. *Phys. Rev. B* **2005**, *71*, 245324.
- (10) Tokumoto, Y.; Shibata, N.; Mizoguchi, T.; Sugiyama, M.; Shimogaki, Y.; Yang, J. S.; Yamamoto, T.; Ikuhara, Y. *J. Mater. Res.* **2008**, *23*, 2188.
- (11) Hawkridge, M. E.; Cherns, D. *Appl. Phys. Lett.* **2005**, *87*, 221903.
- (12) LilienthalWeber, Z.; Chen, Y.; Ruvimov, S.; Washburn, J. *Phys. Rev. Lett.* **1997**, *79*, 2835.
- (13) McCullen, E. F.; Thakur, J. S.; Danylyuk, Y. V.; Auner, G. W.; Rosenberger, L. W. *J. Appl. Phys.* **2008**, *103*, 063504.
- (14) Mattila, T.; Nieminen, R. M. *Phys. Rev. B* **1996**, *54*, 16676.
- (15) Brien, V.; Pigeat, P. *J. Cryst. Growth* **2008**, *310*, 3890.
- (16) Kazan, M.; Nader, R.; Moussaed, E.; Masri, P. *J. Cryst. Growth* **2006**, *290*, 44.
- (17) Edgar, J.; Dua, L.; Nyakiti, L.; Chaudhuri, J. *J. Cryst. Growth* **2008**, *310*, 4002.
- (18) Gorzawski, G.; Sternitzke, M.; Mízzler, W. F.; Berger, A.; Mízzler, G. *J. Eur. Ceram. Soc.* **1995**, *15*, 95.
- (19) Jarrige, J.; Lecompte, J. P.; Mullot, J.; Müller, G. *J. Eur. Ceram. Soc.* **1997**, *17*, 1891.
- (20) Slack, G. A.; Schowalter, L. J.; Morelli, D.; Freitas, J. A. *J. Cryst. Growth* **2002**, *246*, 287.
- (21) Ye, H. G.; Chen, G. D.; Zhu, Y. Z.; Wei, S. H. *Phys. Rev. B* **2008**, *77*, 033302.
- (22) Miao, M. S.; Moses, P. G.; Weber, J. R.; Janotti, A.; Walle, C. G. *V. d. Europhys. Lett.* **2010**, *89*, S6004.
- (23) Ye, H. G.; Chen, G. D.; Wu, Y. L.; Zhu, Y. Z. *J. Appl. Phys.* **2010**, *107*, 043529.
- (24) Arslan, I.; Browning, N. D. *Phys. Rev. Lett.* **2003**, *91*, 165501.
- (25) Elsner, J.; Jones, R.; Haugk, M.; Gutierrez, R.; Frauenheim, T.; Heggie, M. I.; Oberg, S.; Briddon, P. R. *Appl. Phys. Lett.* **1998**, *73*, 3530.
- (26) Perdew, J. P.; Wang, Y. *Phys. Rev. B* **1992**, *45*, 13244.
- (27) Kresse, G.; Furthmuller, J. *Phys. Rev. B* **1996**, *54*, 11169.
- (28) Kresse, G.; Furthmuller, J. *Comput. Mater. Sci.* **1996**, *6*, 15.
- (29) Vanderbilt, D. *Phys. Rev. B* **1990**, *41*, 7892.
- (30) Pack, J. D.; Monkhorst, H. J. *Phys. Rev. B* **1977**, *16*, 1748.
- (31) Mills, G.; Jónsson, H.; Schenter, G. K. *Surf. Sci.* **1995**, *324*, 305.
- (32) Ye, H. G.; Chen, G. D.; Wu, Y. L.; Zhu, Y. Z.; Wei, S. H. *Phys. Rev. B* **2008**, *78*, 193308.
- (33) Ye, H. G.; Chen, G. D.; Wu, Y. L.; Zhu, Y. Z.; Wei, S. H. *Phys. Rev. B* **2009**, *80*, 033301.
- (34) Miao, M. S.; Janotti, A.; Van de Walle, C. G. *Phys. Rev. B* **2009**, *80*, 155319.
- (35) Lymperakis, L.; Neugebauer, J. *Phys. Rev. B* **2009**, *79*, 241308.
- (36) Yan, Y.; Al-Jassim, M. M.; Wei, S. H. *Phys. Rev. B* **2005**, *72*, 161307.